The Vertical Structure of TOGA COARE Convection. Part I: Radar Echo Distributions

CHARLOTTE A. DEMOTT AND STEVEN A. RUTLEDGE

Department of Atmospheric Science, Colorado State University, Fort Collins, Colorado

(Manuscript received 10 September 1996, in final form 15 December 1997)

ABSTRACT

Radar data collected by the 5-cm MIT radar, which was deployed aboard the R/V *Vickers* during the intensive observing period of the Tropical Ocean Global Atmosphere Coupled Ocean–Atmosphere Response Experiment, are partitioned into convective and stratiform Cartesian grid columns. The vertical structure of convective echo is examined through the use of two variables: echo top height and the height of the 30-dB*Z* reflectivity contour. The first of these variables has traditionally been used to describe the vertical structure characteristics of convection, and the second has recently been linked to internal microphysical properties and lightning.

Histograms of the relative frequency of convective-only echo top heights and 30-dB*Z* contour heights were constructed for the three cruises of the *Vickers*, with each cruise experiencing different phases of the intraseasonal oscillation (ISO). Cruise 1, which was dominated by the convectively ''inactive'' phase of the ISO was characterized by the highest frequency of shallow convection (based on echo top heights), whereas cruise 2, which was dominated by a particularly well-defined passage of the convective phase of the ISO, exhibited the tallest echo top heights. Cruise 3 convection was influenced by moderate westerly surface winds characteristic of postwesterly wind burst conditions, and convection was of intermediate height.

When viewed as a function of ''internal'' vertical structure (i.e., 30-dB*Z* contour height), the frequency distributions vary less from cruise to cruise, with cruises 1 and 2 having nearly identical distributions of convective 30-dB*Z* contour heights. Furthermore, when the contribution to convective rainfall is examined as a function of 30-dB*Z* contour height, it is seen that relatively more rain fell from vertically ''intense'' convection (i.e., convection with tall 30-dB*Z* contours) during cruises 1 and 3 than during cruise 2. Instantaneous correlations between rainfall rate and radar echo height were highly scattered about a mean value of about 0.55, whereas rainfall rate and 30-dB*Z* contour height correlations peaked at about 0.8 and exhibited much less scatter.

1. Introduction

Tropical precipitation is an important component of the atmosphere's general circulation because of its role as a heat source for large-scale circulations. Although precipitation occurs at all tropical longitudes, it is concentrated in three preferred longitudinal regions: the Amazon basin, the equatorial regions of the African continent, and the broad Maritime Continent–western Pacific warm pool region, together spanning from approximately 100°E to 160°E. This nonuniform distribution of tropical heating leads to large-scale circulations that are zonally asymmetric, such as the longitudinally oriented Walker circulation, which has its rising branch anchored over the Maritime continent and western Pacific warm pool. The western Pacific warm pool region is a particularly important link in the global circulation because it is characterized by the highest sea surface temperatures and the highest oceanic annual rainfall totals observed anywhere on the globe. This disproportionately large heat source leads to the zonally oriented Walker circulation.

Hartmann et al. (1984) and DeMaria (1995) have demonstrated that the vertical structure of the Walker circulation is sensitive to the vertical distribution of diabatic heating in the tropical troposphere. Furthermore, Lau and Peng (1987) have shown that the phase speed of the 30–60 day intraseasonal oscillation (ISO; Madden and Julian 1994), which may help trigger El Niño events, is also sensitive to the vertical distribution of diabatic heating.

Mesoscale convective systems (MCSs) are the primary source of precipitation and therefore diabatic heating in the Tropics, and are composed of both convective and stratiform clouds. Mesoscale heating (associated with stratiform precipitation) typically enhances the upper-level convective heating but counters lower-level heating through melting and evaporative cooling. To a first approximation, the shape of the overall MCS heating profile is determined by the relative amounts of convective and mesoscale heating, which are proportional to the relative amounts of convective and strati-

Corresponding author address: Dr. Steven A. Rutledge, Department of Atmospheric Science, Colorado State University, Fort Collins, CO 80523.
E-mail: rutledge@olympic.atmos.colostate.edu

form (mesoscale) precipitation. However, convective and stratiform precipitation produce heating profiles that may vary both in magnitude and in the vertical distribution of heating and/or cooling. These variations on the basic MCS convective and stratiform heating profiles will influence the vertical shape of the heating profiles and thus impact the larger-scale circulations. Houze (1989) summarized observations of stratiform heating profiles for MCSs at various stages in their life cycle from several geographic locations. He concluded that mesoscale diabatic heating profiles are not substantially different from one location to the next and suggested that variations in total heating profile shape that could not be explained by relative convective–stratiform rainfall contributions must lie in differences in the vertical distribution of convective heating. Such differences, then, should be closely related to microphysical processes (Tao et al. 1990). For example, convective cells with enhanced ''warm rain'' processes (rainfall produced by collisions-coalescence) should have latent heating concentrated below the freezing level, whereas convective cells with significant ice processes (i.e., riming and/or depositional growth) should provide stronger latent heating above the freezing level.

Observations of the distribution of tropical convective and stratiform rainfall and the vertical distributions of heating associated with MCSs have come primarily through field programs such as the GARP (Global Atmospheric Research Program) Atlantic Tropical Experiment (GATE), the Winter and Summer Monsoon Experiment, the Australian Monsoon Experiment (Holland et al. 1986), the Equatorial Monsoon Experiment (Webster and Houze 1991), the Taiwan Area Mesoscale Experiment (Cunning 1988; Jorgensen and LeMone 1988), the Down Under Doppler and Electricity Experiment (Rutledge et al. 1992), the recently completed Tropical Ocean Global Atmosphere Coupled Ocean–Atmosphere Response Experiment (TOGA COARE; Webster and Lukas 1992), and others. These field programs have provided information on the structure of tropical MCS, their associated heating profiles, and their variability over various spatial and temporal scales.

While some work has addressed the vertical structure of individual convective systems (Szoke et al. 1986; Rutledge et al. 1992; Zipser and Lutz 1994), our knowledge is still incomplete regarding the overall vertical structure of tropical MCSs (i.e., the vertical distribution and phase of both cloud and precipitation particles) and, importantly, how these structures vary with time, for example, over the course of 3–5-day easterly waves, or submonthly variability associated with the ISO.

The purpose of this study is to describe the vertical structure of tropical convective precipitation and its variability with time as observed during the four month intensive observing period (IOP) of TOGA COARE. Part I of this study focuses on monthly mean characteristics of the observed convection and compares the results to similar analyses of GATE data. Part II focuses on factors governing the variability of COARE convection and how this variability may influence diabatic heating profiles. Part I is organized as follows: a brief description of TOGA COARE, the data used in this study, and the methods used to process it are presented in section 2. Results of the analysis and comparisons to GATE distributions are presented in section 3. The results are discussed in section 4, and a summary is given in section 5.

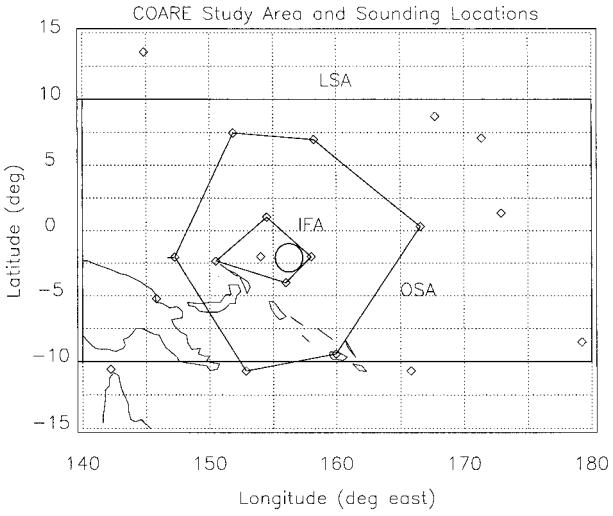

FIG. 1. The TOGA COARE study area. The outer sounding array (OSA), large-scale array (LSA), and intensive flux array (IFA) are shown, as well as the area of MIT radar data used in this study (small circle located within the IFA). The R/V *Vickers* and MIT radar were located at the center of the radar echo coverage circle.

2. Data collection and processing

a. Overview of TOGA COARE

The TOGA COARE IOP was conducted from November 1992 through February 1993. The goals and observing network of TOGA COARE were described by Webster and Lukas (1992). Locations of a subset of these observing platforms are shown in Fig. 1. Chen et al. (1996) analyzed the time series of infrared brightness temperature during the IOP, and Lin and Johnson (1996) analyzed data from the COARE sounding network to describe synoptic conditions and variability in the COARE study area. Three passages of the ISO were observed during the IOP, with the most clearly defined passage occurring in late December 1992 to early January 1993. Lin and Johnson presented a schematic of the ISO based upon the three passages during COARE (see their Fig. 16), which are discernible in the wind speed, rainfall, and mean vertical motion time series of Fig. 2. During the inactive phase of the oscillation, 1000-mb winds and tropospheric shear are weak. As the convective phase approaches from the west, surface easterlies increase slightly and are accompanied by an increase in tropospheric shear. Following the passage of

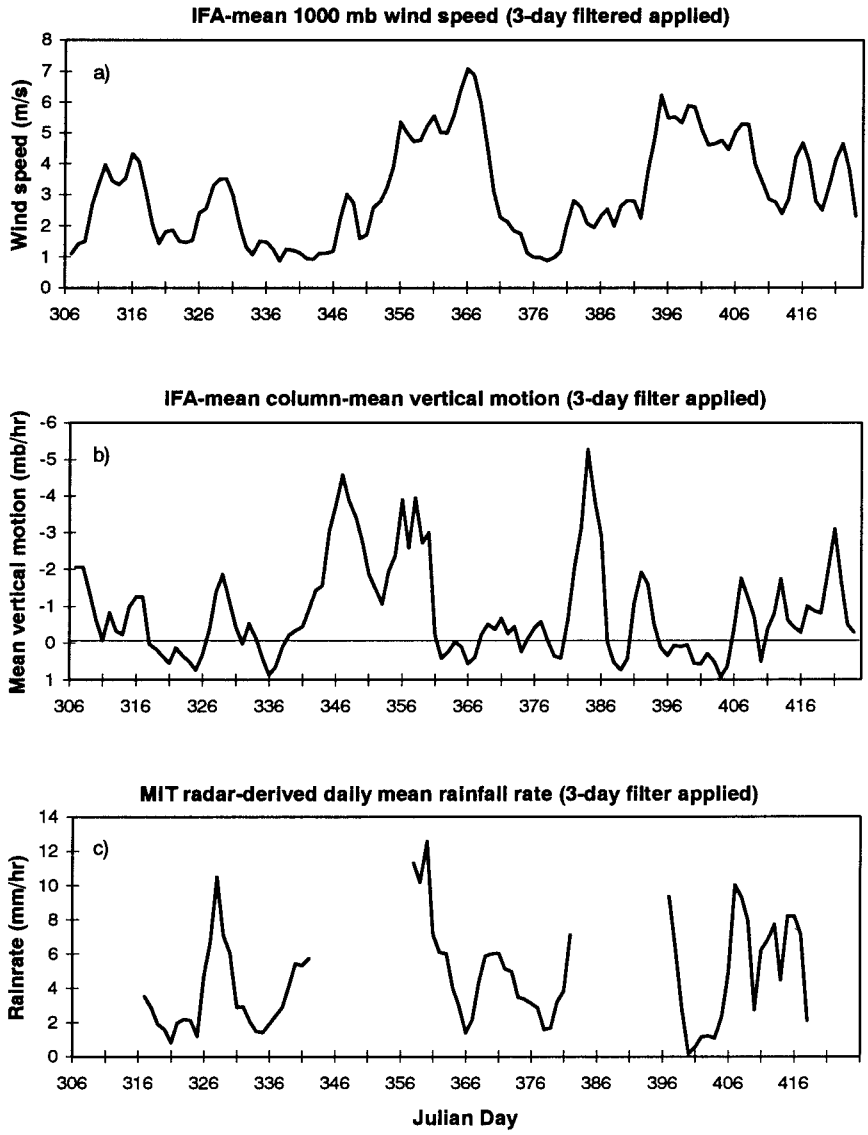

FIG. 2. Time series of (a) daily mean surface wind speed, (b) column mean vertical motion, and (c) MIT radar-derived rainfall. Surface wind speed and vertical motion curves are based on the objective sounding analysis described in Lin and Johnson (1996) for the IFA.

intense convective activity, surface winds become westerly and frequently more than twice as strong as their easterly counterparts. This is commonly known as the westerly wind burst (WWB). Tropospheric shear is highest during WWB events and may exceed 50 m s^{-1} over the depth of the troposphere. WWBs are often marked by a noticeable suppression of convective activity during their passage. As the active phase of the oscillation propagates farther east, the surface westerlies decrease and eventually revert to weak easterlies.

b. Radar data processing

As part of the COARE observing network, two 5-cm Doppler radars were operated on research ships and deployed to locations within the intensive flux array (IFA) for three 30-day periods. The Massachusetts Institute of Technology (MIT) radar was deployed aboard the *John V. Vickers*, and the nearly identical TOGA radar was deployed aboard the PRC ship *Xiangyonghang No. 5*. Characteristics of the MIT radar, which is the primary data source of this study, are summarized in Table 1. Additional radar details, including a description of the stabilization method used can be found in Rutledge et al. (1993). Dates of the three cruises of the *Vickers* are listed in Table 2, as well as a brief summary of the weather conditions sampled during each cruise.

When deployed to its ''fixed position'' (2.08°S, 156.25°E), the MIT radar operated continuously in both surveillance and full-volume scanning modes. The ship

TABLE 1. Characteristics of the MIT C-Band radar.

Operating frequency	5590 MHz
Minimum detectable signal	−115 dbm
Peak power	155 kW
Pulse width	1.0 μs
Antenna gain	40.5 dB
Beamwidth	1.6° (3 dB)
Elevation upper limit	50°
Elevation lower limit	−18°
Pulse repetition frequency	250–1500 Hz

was allowed to drift no more than 15 km from this location. This resulted in repositioning approximately twice per day. The scanning strategy of the radar was such that a surveillance scan and a full volume scan were collected every 10 min. In this study, every other radar volume was analyzed, yielding just over 6100 full volumes at a temporal resolution of 20 min. Raw polar data were interpolated onto a 240 km × 240 km × 18.5 km Cartesian grid (centered on the fixed position, rather than on the variable ship position) with grid spacing of 2 km × 2 km × 0.5 km using the National Center for Atmospheric Research's REORDER software.

c. Identification and description of convective echo

Once interpolated to a Cartesian grid, the radar data were partitioned into convective and stratiform components using a technique based upon Steiner and Houze (1993). This technique separates radar reflectivity data into convective and stratiform echo populations based on 1) the magnitude of reflectivity at a Cartesian data point and 2) the horizontal reflectivity gradient surrounding a local reflectivity maxima. While Steiner and Houze (1993) applied such criteria to a vertical level close to the surface and sufficiently below the freezing level to avoid contamination from brightband effects, the modifications to this approach used in this study allow the partitioning to be applied at *all* vertical levels in an effort to better resolve tilted convection in a sheared environment. The modifications to this algorithm are described more completely in the appendix but essentially consist of modifying the convective reflectivity threshold based on the distribution of reflectivity data at $z = 2$ km height. The goal of this modification was to include more small developing and aging convective cores in the convective partition. The effect of this modification is similar to that achieved by the ''variable reflectivity difference'' curve presented in the revised Steiner and Houze (1993) partitioning algorithm [see Fig. 7 of Steiner et al. (1995)].[1] The algorithm was tested and refined by making numerous subjective comparisons of vertical cross sections, as well as by measuring the width of contoured frequency by altitude diagrams (CFADs; Yuter and Houze 1995) of stratiform vertical velocities (obtained from dual-Doppler analyzed winds from both tropical and midlatitude MCSs). These tests indicated that the algorithm performs quite well under a variety of echo situations.

Subsequent modifications of the Steiner and Houze (1993) algorithm have been made by Steiner et al. (1995). These modifications tend to reduce the total convective areas and convective rainfall amounts. Sensitivity tests were performed on several of the assumptions used in both the Steiner and Houze (1993) and Steiner et al. (1995) algorithms. We found that slight differences in arguably subjective but nonetheless reasonable assumptions can change convective rainfall amounts by as much as 15% (T. Rickenbach 1996, personal communication). For example, using the same radar dataset as examined in this study, different sets of partitioning assumptions resulted in COARE mean convective rainfall fractions ranging from 65% to 80% of the total rainfall. Convective rainfall fractions using the partitioning technique described in the appendix yield convective rainfall fractions near the upper limit of this range.

Rainfall rates were computed from the partitioned reflectivity data at an altitude of 2 km. Ideally, only the lowest levels of radar data should be used to diagnose rainfall, but selecting a 2-km height permitted rain mapping to a range of 120 km from the radar. Subsequent to our analysis, Kucera et al. (1996) suggested a revision to the *Z–R* relations used in this paper based on their finding that the volume average convective reflectivity profiles in COARE increased slightly from the 2-km altitude to the surface. However, early analysis per-

[1] Unlike the Steiner et al. (1995) algorithm, we do not use a variable cell radius, so convective rainfall totals and areas are somewhat greater than what would be obtained with their algorithm. Comparisons between the two algorithms suggest a mean difference in the percentage of convective rainfall of about 5%.

TABLE 2. Dates of the three cruises of the R/V *Vickers* during TOGA COARE.

Cruise	Dates	Julian days*	Weather synopsis
1	10 Nov 1992–10 Dec 1992	315–345	Dominated by light surface winds; inactive phase of ISO
2	21 Dec 1992–19 Jan 1993	356–385	Sampled the most intense convective and WWB phases of the three ISOs, then 1 week of inactive phase
3	29 Jan 1993–25 Feb 1993	395–412	Weather dominated by convection associated with constant westerly surface flow

* For 1993 dates, 366 has been added to the Julian day.

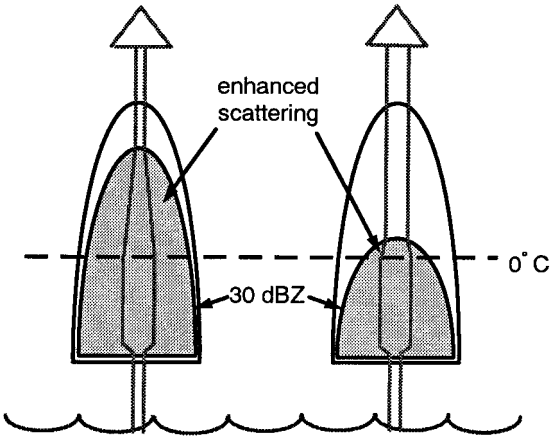

FIG. 3. Schematic illustration of two convective features interacting with upwelling 85-GHz radiation (radiant energy at this frequency is proportional to the width of the open gray arrows). The features are the same height yet have different internal structures. The left-hand feature has a higher 30-dB*Z* contour that the right-hand feature, corresponding to greater liquid and ice water masses above the freezing level. Because ice is a strong scatterer at 85 GHz, the left-hand feature produces a lower 85-GHz brightness temperature than the right-hand feature.

formed by the authors of this paper revealed a wide variety of mean convective reflectivity profile shapes for individual convective features (based on partitioned echo). Many convective features, particularly the smaller, more isolated convective cells, *do not* exhibit the slight increase in reflectivity below the 2-km level that is seen in the volume mean profile. Since our analysis is based on small-scale measurements (2 km × 2 km grid columns), we felt that any uniform correction to the reflectivity used to compute rainfall totals would be inappropriate.

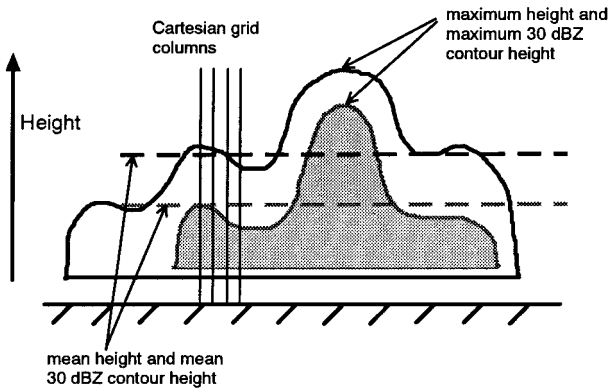

FIG. 4. Schematic vertical cross section of a convective feature composed of four convective cells. The black curve corresponds to the echo boundary; the gray curve corresponds to the 30-dB*Z* contour. Reflectivity greater than 30 dB*Z* is shaded in light gray. Convective feature heights, 30-dB*Z* contour heights, and rainfall associated with convective features categorized by their *maximum* height may be several kilometers higher than their *mean* heights (heavy dashed lines). An alternative method of describing convective echo is to record the height, 30-dB*Z* contour height, and rainfall of each Cartesian grid column, samples of which are illustrated by thin vertical lines.

Based on the analysis of disdrometer data from Kapingamarangi Atoll during COARE by Tokay and Short (1996), two separate *Z–R* relationships were used to compute rainfall from convective and stratiform echo. For convective echo, the relationship used was $Z = 139R^{1.43}$ and for stratiform echo, $Z = 367R^{1.30}$ was applied. While the difference in rainfall rates arising from the two *Z–R* relations is large, we feel that they are a true representation of the physical differences between convective and stratiform rainfall. Furthermore, these relationships were derived from disdrometer data collected within the IFA, so they are the most appropriate relationships to use in this study.

Once the data were partitioned into convective and stratiform components, attention was turned to developing a method to accurately depict the vertical structure of convective echo. The vertical structure of a population of radar echoes has most often been described by echo top height (e.g., López 1977; Houze and Cheng 1977; Leary 1984). However, there exist ''internal'' variations in vertical structure that cannot be accounted for with an echo top height only classification. A schematic illustration of such variability is presented in Fig. 3. This figure depicts two oceanic convective cells with the same echo height, but different internal structures, as suggested by the 30-dB*Z* contour heights. Because the two cells have identical heights, they would have the same IR brightness temperature. However, their microwave emission characteristics would be quite different. As Zipser (1994) and Petersen et al. (1996) have pointed out, the presence of ≥30-dB*Z* reflectivity above the freezing level is often associated with lightning production and presumably larger supercooled water and ice water contents. Since ice is a strong scatterer at high microwave frequencies (e.g., 85 GHz), the left-hand cell in Fig. 3 would have a lower 85-GHz brightness temperature than that observed from the cell on the right. These differences in internal structure may also reflect differences in updraft velocities, and thus heating rates, which is the subject of Part II of this study. Because both echo top height and 30-dB*Z* contour height vary from cell to cell, convective echo as identified by the partitioning algorithm will be described both in terms of echo top height (defined as the 0-dB*Z* reflectivity contour in this study) and 30-dB*Z* contour height (when reflectivity of this magnitude is present).

A second component of determining how to describe convective echo is the consideration of horizontal characteristics. As precipitating systems become more organized, their individual convective cores tend to become closely spaced, so that when the partitioning algorithm is applied, several convective cores are often grouped together into a single convective feature, which is defined for the purposes of this study as a group of one or more convective cells contiguously connected by at least one side of one Cartesian grid box. Figure 4

presents a schematic illustration of a vertical cross section of a convective feature composed of several convective cores. As is typically done in this type of study (e.g., López 1977; Houze and Cheng 1977; Leary 1984), the height of the feature is determined by the height of the tallest grid column within that feature, even though this height may be representative only of a single convective core within that feature. This same bias will be present when this method is used to compute 30-dB*Z* contour heights. The average feature height and 30-dB*Z* contour height, shown by the heavy dashed lines in Fig. 4, are also not particularly representative of any of the individual cores contained within the feature.

An additional drawback to the ''feature'' approach of computing heights is the tendency for the tallest height bins to be overrepresented in calculations of the contribution to total convective area and rainfall. In other words, in the feature illustrated, precipitation is produced from convection of multiple heights, but because the cores are all connected, all of the rainfall produced by this feature would be classified as being produced by the tallest core. Furthermore, the degree to which individual convective cores are merged together to form convective features is quite sensitive to the assumptions concerning cell radius in the partitioning algorithm. Therefore, differences in partitioning assumptions, or ''tuning,'' may yield different results in an analysis of convective echo top heights or 30-dB*Z* contour heights.

An alternative approach to describing convection utilizes Cartesian ''grid columns'' and focuses on the ''texture'' of convective echo rather than the size of individual features. In this approach, echo top height, 30-dB*Z* contour height (when present) and rainfall rate are determined for each grid column of convective echo, thereby eliminating the complicating factors of feature area. Furthermore, while this approach does not eliminate the sensitivity to partitioning assumptions, it greatly reduces it, since a large number of the grid columns that are classified as convective with one set of partitioning assumptions will also be classified as convective using another set of assumptions (i.e., different assumed convective radii).

The grid column approach has a disadvantage in the uncertainty that convective rainfall observed at the 2-km level was produced by processes taking place at higher levels in the same grid column. For example, in the 2 km $\times$ 2 km horizontal grid spacing used in the study, even the slightest wind shear can advect raindrops or ice particles through several grid columns over a depth of just a few km. Because of this, rain falling through the 2-km level should be thought of as being ''associated with,'' rather than ''produced by'' a grid column with certain height characteristics. In contrast, stating that rainfall is produced by a convective feature is physically reasonable, since it is unlikely that a large portion of the rain falling underneath a convective feature was advected from a location beyond the feature limits.

The analysis described in the next section was performed for both convective features and convective grid columns. However, because the grid column analysis is less sensitive to partitioning assumptions, we will focus on the grid column distributions of convective echo in this work. In the few cases where results are presented in terms of convective feature distributions, it should be kept in mind that the results may be different using a different set of assumptions when performing the partitioning.

3. Results

From a statistical point of view, production of convective rainfall as a function of echo top height depends on the number and mean rainfall rate of convective grid columns within a given height bin. The purpose of this section is to examine the distribution of convective echo in terms of two measurements: 1) the height of convective echo as inferred from the minimum radar reflectivity and, 2) the ''vertical intensity'' of the convective echo as inferred from the maximum height of the 30-dB*Z* reflectivity contour. These statistics will be presented for each 30-day cruise of the *Vickers,* as each cruise sampled somewhat different large-scale weather conditions. The contribution to total convective rainfall and the range of rainfall rates encountered for each echo top and 30-dB*Z* height bin are also examined.

a. One-dimensional echo distributions and contributions to convective rainfall

Cruise-mean frequency distributions of 1) echo top height and 2) 30-dB*Z* contour height based on convective grid columns are presented in Fig. 5. During the first cruise, which occurred during the convectively ''inactive'' phase of the ISO and was characterized by the greatest number of days with unorganized convective activity (Rickenbach and Rutledge 1998), the largest percentage of echo top heights are found in the 4–5 and 5–6 km height bins, with the percentages dropping off steadily with increasing height. In contrast, cruises 2 and 3 were characterized by more days of organized precipitation associated with the convectively active phases of the ISO and have distribution peaks in the 7–8-km height bins. Cruises 2 and 3 have the highest number of pixels in ''tall'' height bins, with 59% and 63%, respectively, of pixels being taller than 7 km compared to 53% for cruise 1.

The distributions of 30-dB*Z* heights for all three cruises, shown by shaded bars in Fig. 5, are all approximately normal and peak in the 4–5-km height bin. However, there are as many ''vertically intense'' convective grid columns, as evidenced by the 30-dB*Z* contour height, during cruise 1 (53% taller than 4 km) as during cruise 2 (53%) and nearly as many for cruise 3 (56%). Therefore, it appears that, even though convective cells observed during cruise 1 were relatively shallow, they

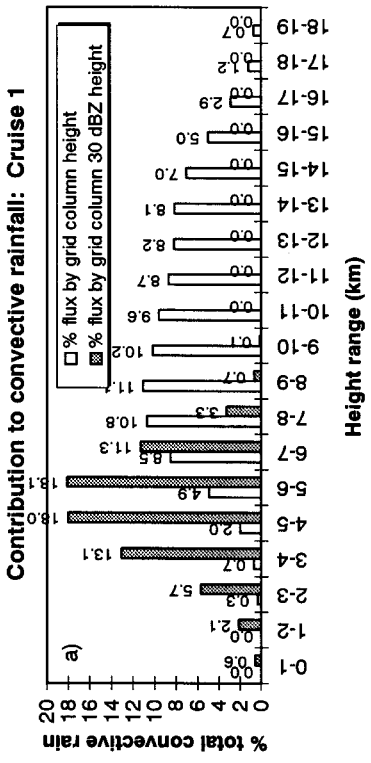

FIG. 6. Relative contribution to total convective rainfall by convective grid column heights (open bars) and convective grid column 30-dBZ contour heights (shaded bars) for cruises 1, 2, and 3.

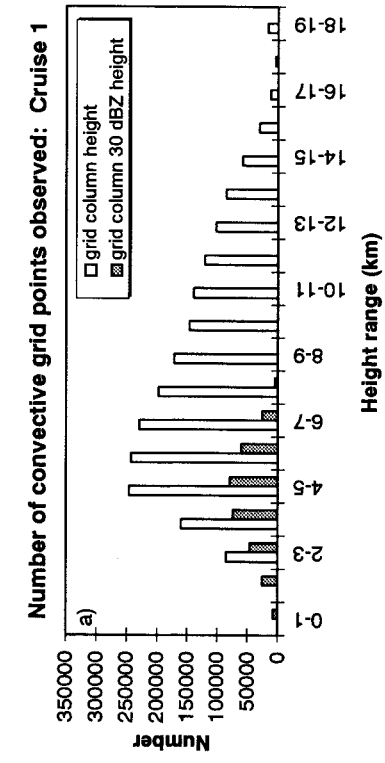

FIG. Fig. 5. Frequency distribution of convective grid column heights (open bars) and convective grid column 30-dBZ contour heights (shaded bars) for cruises 1, 2, and 3.

were characterized by total water contents above the freezing level (approximately 4.5 km during COARE) as high as those observed for the deeper cells (defined by overall echo depth) of cruises 2 and 3. In contrast, the convective cells of cruise 2 were tall, but on average had less than or the same total water mass above the freezing level compared to the shallower cells of cruise 1. Physically, this implies that convective ''vigor,'' as indicated by either elevated water mass or vertical velocity (which is required to maintain an elevated water mass), does not necessarily scale with echo top height.

To an extent, the distributions of convective rainfall contribution as a function of height (Fig. 6) reflect the number distributions in Fig. 5. However, a disproportionate amount of rainfall is accounted for by the taller height bins, reflecting the fact that deeper convection tends to produce heavier precipitation than shallower convection (Leary 1984). The rainfall distributions as a function of echo top height are quite broad in both cruises 1 and 2 and both peak at the 8–9-km height bin. However, the rainfall distribution for cruise 1 is nearly bimodal; the ''flat'' part of the distribution in the 12–14-km height range and the true peak in the 8–9-km height range suggest the presence of two rain-producing cloud populations. Evidence of these two populations is seen more clearly in rainfall distributions based upon (instantaneous) feature top height (DeMott 1996; not shown). The rainfall distribution for cruise 3 is more peaked than it is for either cruises 1 or 2, but the peak occurs at nearly the same altitude. Because the rainfall distribution peaks at taller height bins than does the frequency distribution of echo tops for the three cruises, rainfall rates must increase with increasing height, as is examined in section 3c.

The fact that the grid column rainfall distributions peak at relatively low levels may come as a surprise when compared to similar results for GATE. For example, Cheng and Houze (1979) found that convective rainfall contribution peaked for cores in the 12–13-km height range (for convection that did not ''overshoot'' its level of neutral buoyancy). The discrepancy between these two analyses lies with the fact that the Cheng and Houze study was based on convective features, whereas the results in Figs. 5 and 6 are based on convective grid columns. A more direct comparison between COARE and GATE rainfall distributions may be made by looking at the cruise 3 rain distributions as a function of feature height (as opposed to grid column height), which is presented in Fig. 7. The cruise 3 distribution is shown since it lies roughly between those of cruises 1 and 2 and closely resembles the COARE IOP mean distribution. We should note that this figure cannot be treated as a truly direct comparison, since the GATE results [obtained from Cheng and Houze (1979)] are based on maximum echo height, whereas the COARE results are based on instantaneous echo heights. This difference accounts for the distribution ''notch'' in the GATE data, which arises from cells that do and those that do not overshoot their level of neutral buoyancy. The bias toward taller heights in the feature analysis discussed in section 2 is immediately obvious; the rainfall contribution now peaks at 15–16 km, which is higher than the GATE peak (Fig. 7b) but consistent with the higher tropopause in the western Pacific warm pool region (approximately 16 km) compared to that of the eastern Atlantic (approximately 13 km).

Rainfall contribution as a function of 30-dB*Z* contour height remains approximately normally distributed, peaking in the 5–6-km height bin for all three cruises (see Fig. 6). However, close inspection of these distributions reveals that relatively more rain fell from grid columns with 30-dB*Z* contours taller than 5 km during cruise 1 (34%) than did in either cruise 2 (27%) or cruise 3 (32%). Therefore, there are distinct differences in rainfall production as a function of vertical structure for each of the three cruises, particularly between cruises 1 and 2. Namely, rainfall production as a function of echo top height during cruise 1 was dominated by relatively shallow echo tops, whereas cruise 2 rainfall production was shifted toward echoes with higher tops. Conversely, when viewed as a function of 30-dB*Z* contour height, the taller 30-dB*Z* height echoes of cruise 1 produced comparatively more rain than they did during cruise 2 (note also Table 3). This discrepancy between ''external'' (echo top height) and ''internal'' (30-dB*Z* contour height) structure of convection urges the use of caution when making assumptions about rainfall production mechanisms based only upon echo top or cloud-top height.

b. Two-dimensional echo distributions and contributions to convective rainfall

Whereas the previous subsection examined convective echo as a function of either echo top height or 30-dB*Z* contour height, this section considers both variables simultaneously, in an effort to illustrate the wide variety of internal convective structures for convective grid columns of the same height. For each grid column containing a reflectivity value of at least 30 dB*Z* somewhere in the column, a point can be plotted on an echo top height–30-dB*Z* contour height set of axes. This procedure was performed for each such grid column for each cruise. The results are presented in Fig. 8. Since the number of data points is so large, the percentage of total data points contained in each height–30-dB*Z* height bin is contoured in order to produce a clearer picture. The contours may also be thought of as corresponding to the ''density'' of data points on the plot.

Several features of Fig. 8 merit discussion. First, the 2D distributions of convective echo are quite similar for all three cruises; they peak in the 6–9-km echo top height and 3–5-km 30-dB*Z* height bins, in agreement with the 1D distributions presented in the previous subsection. Furthermore, nearly every possible vertical structure (echo top–30-dB*Z* height combination) is pres-

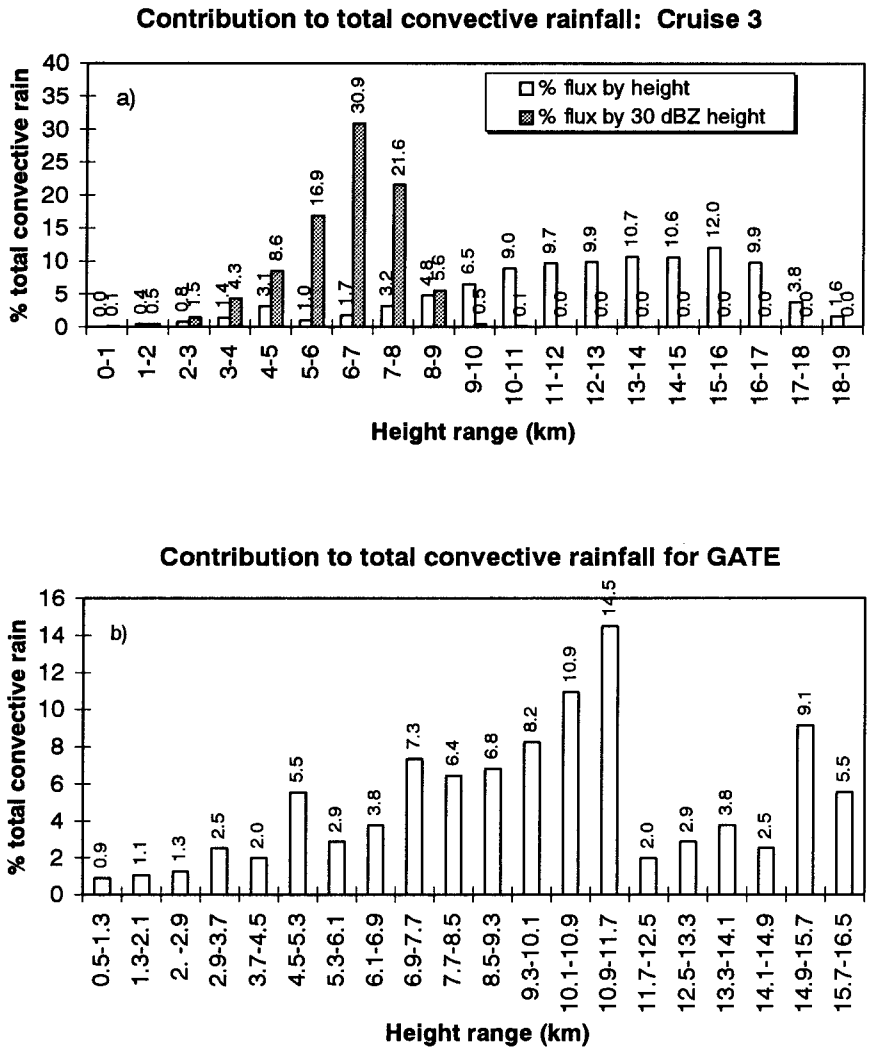

FIG. 7. As in Fig. 6c but for convective feature heights and 30-dBZ contour heights. Figure 7b is based on data presented in Houze and Cheng (1977).

ent to some degree during all of the cruises. In other words, convective echo spans nearly the entire range of possible height–30-dBZ height combinations over monthly timescales.

Cruise-to-cruise differences in the 2D distributions are subtle. First, consider the envelope of grid columns contained within the 1% contour. By computing the percentage of grid columns 10 km tall or less and falling within the 1% contour, it is seen that grid columns with typical 30-dBZ contour heights (1–6 km) are more concentrated in shallow convection during cruises 1 (39% of the total) and 3 (44%) than during cruise 2 (32%). Second, by examining the shape of the 0.01% contour (defining the extrema of the 2D distributions), it appears that convective grid columns with echo top heights in the 5–18-km range during cruise 1 were just as likely to have tall 30-dBZ contour heights as their cruise 2 and 3 counterparts. This point is made clearer by computing the percentage of grid columns with heights greater than 5 km and 30-dBZ heights greater than 5 km. Seventeen percent of cruise 1 grid columns fell into this region, compared to 18% for cruise 2 and 23% for cruise 3. These two comparisons suggest that 1) the

TABLE 3. Relative frequency and convective rainfall contribution by convective columns with 30-dBZ contour heights.

Cruise	Fraction of convective grid columns with 30-dBZ contour heights (%)	Fraction of convective rainfall produced by columns with 30-dBZ contour heights (%)
1	15.9	73.1
2	14.8	66.7
3	16.0	69.1

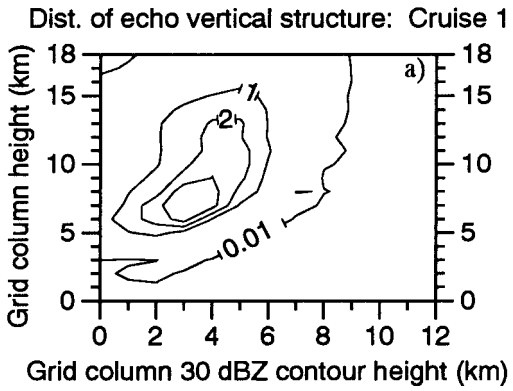

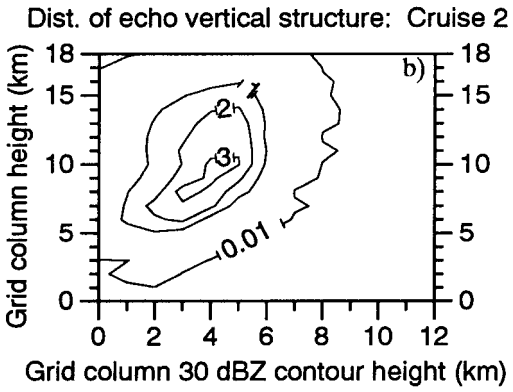

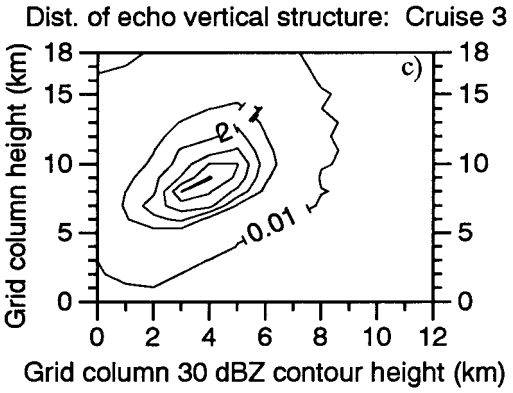

FIG. 8. Relative frequency distribution of convective grid columns as a function of height and 30-dBZ contour height for each of the three cruises of the R/V *Vickers*. Contours correspond to the percentage of grid columns accounted for in each echo top height–30-dBZ height bin.

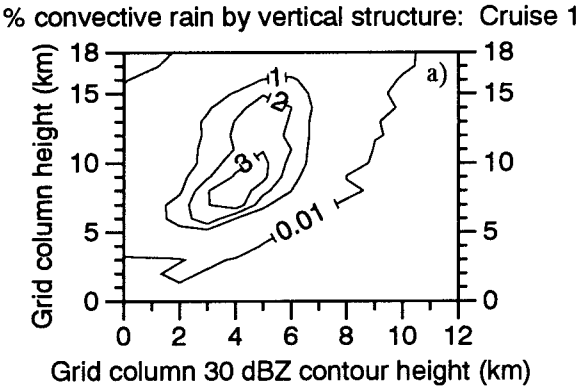

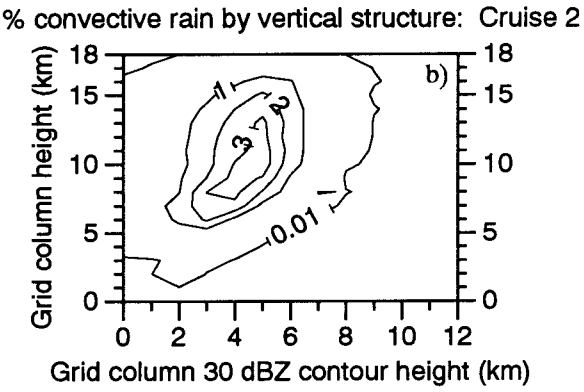

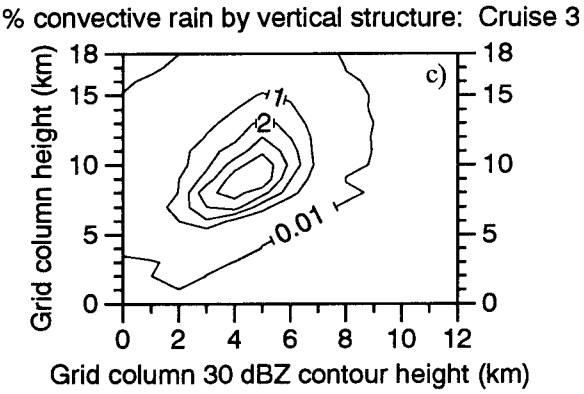

FIG. 9. As in Fig. 8 but for relative contribution to total convective rainfall.

shallower convection of cruise 1 was not necessarily less ''vertically intense'' (as is evident from the 30-dBZ contour heights) than that of cruises 2 and 3, and 2) for a wide variety of cell heights, maximum attainable 30-dBZ heights were similar for all three cruises.

Two-dimensional distributions of convective rainfall are shown in Fig. 9. Again, during cruise 1, rainfall was dominated by echo that was relatively shallow, but had 30-dBZ heights similar to those observed during cruises 2 and 3. By computing the percentage of total rainfall originating from grid shallow grid columns (heights less than 10 km) with 30-dBZ heights 5 km or greater, it is seen that 22% of convective rainfall was produced by this ''shallow but intense convection'' during cruise 1 compared to 17% during cruise 2. Cruise 3 had the greatest fraction of rain produced from this type of convection (27%). These computations emphasize that, despite similarities in echo top height, there may be a wide variety of vertical distributions of rainfall rates, hydrometeor types, and diabatic heating profile shapes for convective cells of similar heights.

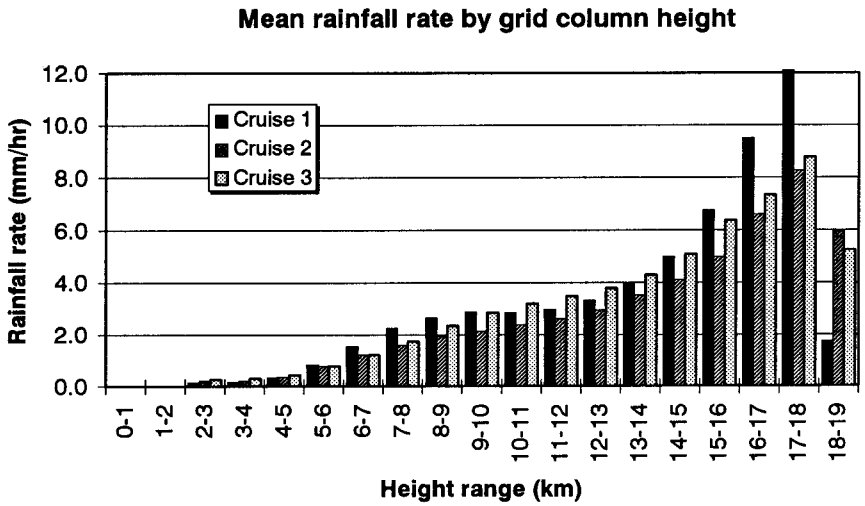

FIG. 10. Mean rainfall rates for convective grid columns as a function of echo top height for cruises 1, 2, and 3. Mean rainfall rates were computed by averaging all 2 km × 2 km pixel rainfall rates having the same echo top (grid column) height.

c. Convective vertical structure and rainfall rates

In this section we examine how variations in convective vertical structure relate to surface precipitation rates. It is important to understand these relationships since, particularly over remote tropical regions, surface rainfall rates are inferred from quantities pertaining to cloud structure far from the surface, such as IR brightness temperature. Cruise-mean surface rainfall rate as a function of grid column echo top height and 30-dBZ contour height are shown in Figs. 10 and 11, respectively. Not surprisingly, the cruise-mean rainfall rates increase with increasing echo top height. These results are similar to those presented by Leary (1984) for GATE convection, although the rainfall rates are approximately twice as high as those in her analysis since Fig. 10 is based on grid column rainfall rates rather than convective feature area mean rainfall rates.

There are two likely causes for the anomalous decrease in rainfall rate for echo tops in the 18–19-km height range. The first reason may be linked to radar beam sidelobe effects, in which intense convection located close to the ship was detected by the radar's sidelobes at high scanning elevation angles. During such conditions, the main radar lobe may have topped the convective core, but sidelobe detection would artificially increase the height of the convection. This behavior was most common when a strong cell was within about a 40-km radius from the ship and only affected less than 6% of all analyzed volumes. Another possible explanation for the decreasing rainfall rates in the tallest

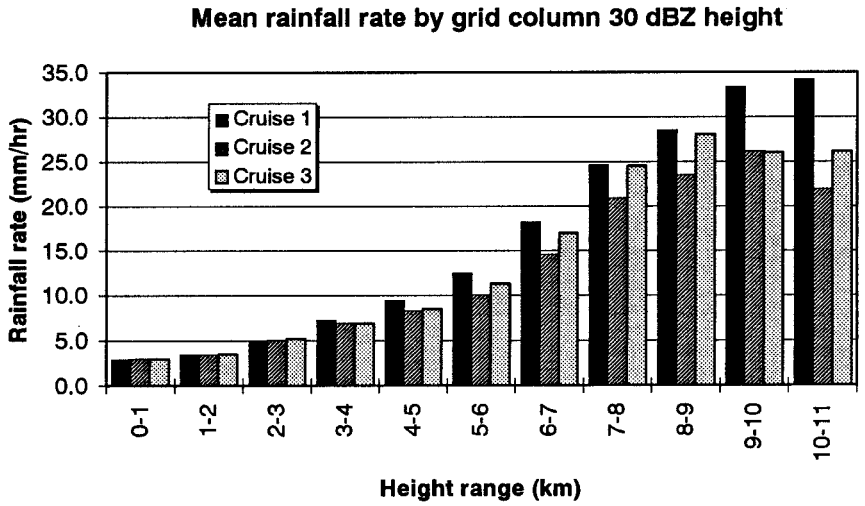

FIG. 11. As in Fig. 10 but for grid column 30-dBZ contour heights.

height bins is that, because of vertical wind shear, the tallest grid columns may not have always been situated directly over the highest 2-km rainfall rates.

Note that in the 5–9-km height bin, cruise 1 rainfall rates were higher than those of cruise 2 and cruise 3, illustrating the fact that even though much of the convection of cruise 1 was rather shallow, it was capable of producing rainfall rates more typical of deeper convection. Furthermore, it is also seen that the relatively tall echo heights observed during cruise 2 produced comparatively weak rainfall rates, suggesting that even on monthly timescales, there is variability in the echo top height–rainfall rate relationship.

Cruise-mean rainfall rate as a function of 30-dB*Z* contour height (Fig. 11) follows a trend similar to that for echo top height. Also, note the tendency for cruise 2 rainfall rates to be the lowest of the three cruises. This fact may be used to address a question relating to the partitioning algorithm applied to the dataset. Namely, one might wonder if the low rainfall rates as a function of echo top height during cruise 2 (Fig. 10) are a consequence of contamination by weaker stratiform rainfall rates during this cruise (cruise 2 was characterized by greater stratiform rainfall amounts and areas than either cruise 1 or cruise 3; Rickenbach and Rutledge 1998). By eliminating grid columns with reflectivities less than 30 dB*Z* (which is where most of the subjectivity involved in the partitioning lies), we are essentially examining convective ''core'' grid columns. Because the trends in rainfall rate as a function of 30-dB*Z* contour height are the same as those for echo top height (i.e., cruise 2 rates are overall less than either cruise 1 or cruise 3), we can be confident that the lower convective rainfall rates observed during cruise 2 are not purely a consequence of stratiform contamination.

Despite the minor cruise-to-cruise differences in rainfall rate as function of height (average height bin difference between cruise 1 and cruise 2 rainfall rates is 21%), the trend of rainfall rate increasing with increasing height is repeated through each cruise. Indeed, this is the physical basis for monthly rainfall retrieval algorithms based on infrared brightness temperature (i.e., Adler and Mack 1984; Arkin and Meisner 1987; Adler and Negri 1988). It is of interest, however, to examine how well the rainfall rate–echo top height (or 30-dB*Z* contour height) applies to shorter timescales.

To investigate this issue, contoured scatter diagrams (similar to those produced in Figs. 8 and 9) were constructed of the population of echo top height–rainfall rate pairs and 30-dB*Z* contour height–rainfall pairs for each of the three cruises. The results of this analysis are presented in Figs. 12 and 13. Although the general increase in rainfall rate with echo top and 30-dB*Z* contour height is apparent in these two figures, the most striking result is the large spread of data points about the ''axis'' of maximum frequency. The distribution is broader for echo top height compared to 30-dB*Z* contour height, suggesting that rainfall estimates based on echo top height over short averaging periods (i.e., daily or even instantaneous estimates) will not be as robust as estimates based on either monthly averaged echo top height *or* on shorter-term averages of 30-dB*Z* contour height.

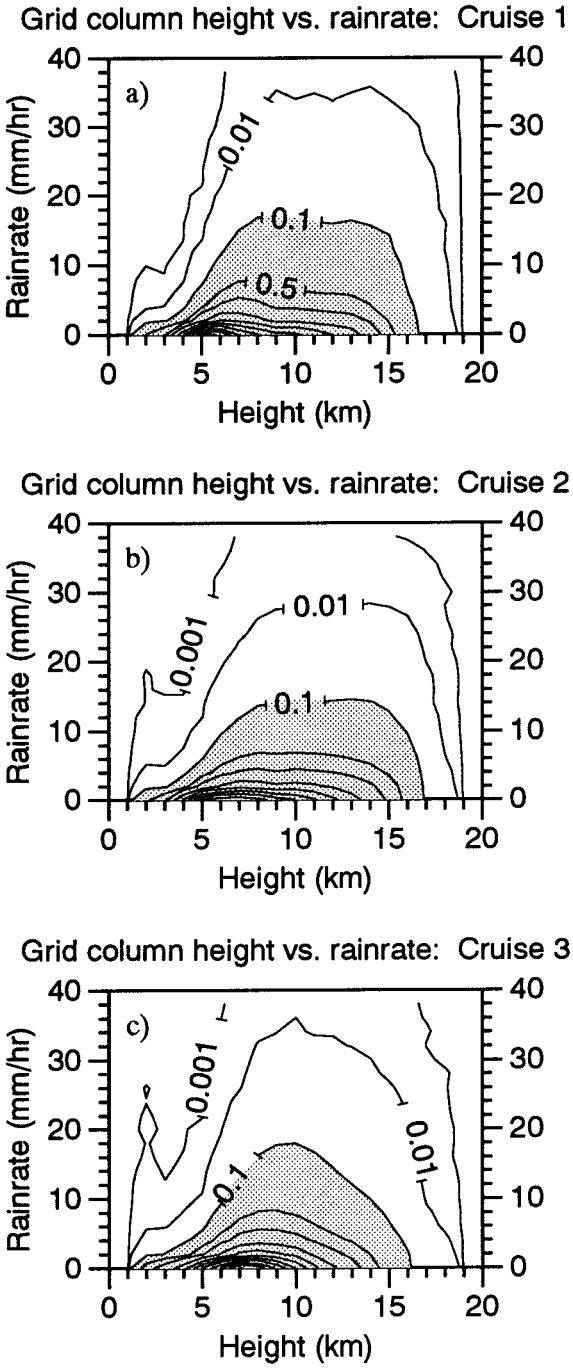

FIG. 12. Relative frequency distribution of convective grid column rainfall rates as a function of grid column echo top height. The contours correspond the percentage of total grid columns falling into each echo top height–rainfall rate bin.

An analysis of instantaneous (i.e., single radar vol-

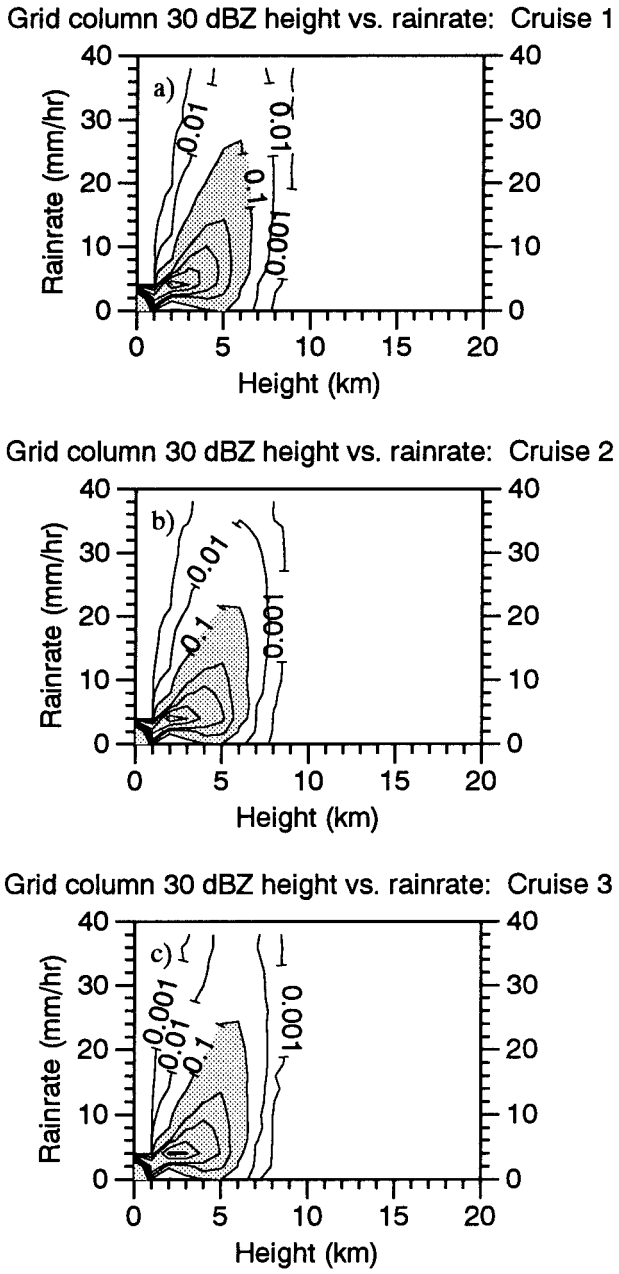

FIG. 13. As in Fig. 12 but for convective grid column 30-dBZ contour height.

ume) rainfall rate–echo top height and rainfall rate–30-dBZ contour height correlations for all analyzed volumes reveals that this is indeed true. The distribution of instantaneous correlations between convective grid column height and 2-km rainfall rate and 30-dBZ column height and 2-km rainfall rate for all three cruises are shown in Fig. 14. Rain-echo top height correlations span a broad distribution and peak in the 0.5–0.6 bin. These relatively low correlations do not appear to be a consequence of sheared convection, since a comparison of Fig. 12a (the low-shear regime of cruise 1) to Fig. 12b (the high shear regime of cruise 2) reveal very little difference in the distribution of rainfall rate–echo top height pairs. Therefore, it appears that such correlations are already low without the complicating factor of shear.

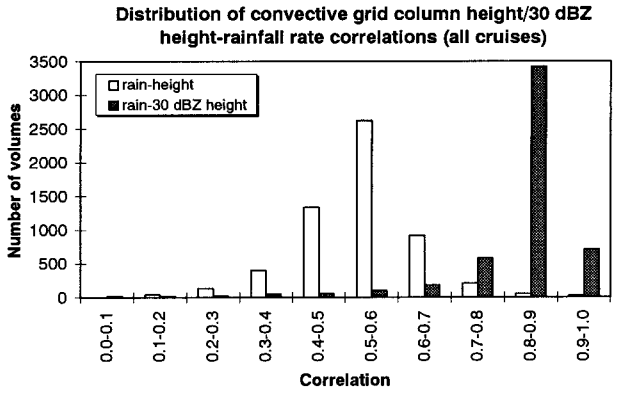

FIG. 14. The distribution of individual radar volume correlations between rainfall rate and grid column echo top height (open bars) and rainfall rate and grid column 30-dBZ contour height (shaded bars). For each radar volume analyzed, a rain rate vs height (or 30-dBZ contour height) correlation was computed. This figure represents the range of correlation coefficients obtained from all 6000+ volumes analyzed over cruises 1, 2, and 3.

Rain–30-dBZ height correlations offer a dramatic contrast. The distribution is strongly peaked in the 0.8–0.9 bin. In fact, 91% of all volumes had correlations equal to or greater than 0.7. On the other hand, there is a long tail of the rain–30-dBZ contour height distribution toward lower correlations. A comparison of the time series of daily mean and minimum rainfall rate–30-dBZ contour height correlations (Fig. 15) suggests that the very low correlations are not entirely uniformly distributed throughout the analysis period, but tend to occur during periods of either high surface winds or widespread convection. Those very low correlations that occur during periods of very high winds (see Fig. 2) are the result of anomalously high sea clutter (arising

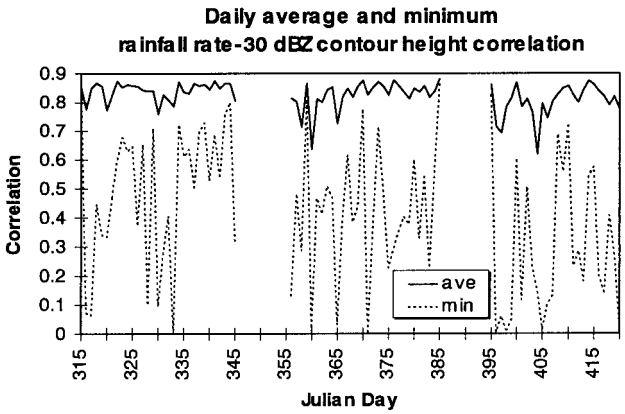

FIG. 15. Time series of the daily mean rain rate–30 dBZ contour height correlation (solid line) and daily minimum rain rate–30 dBZ contour height correlation (dotted line).

TABLE 4. Means and standard deviations of the logarithms of maximum echo height (GATE) and instantaneous feature height (COARE). Gate values obtained from Houze and Cheng (1977).

Vickers cruise or GATE phase	GATE (values from HC)		COARE	
	Mean	Standard deviation	Mean	Standard deviation
1	0.55	0.17	0.72	0.27
2	0.61	0.24	0.75	0.27
3	0.63	0.21	0.72	0.28

from Bragg scattering of the radar beam from the ocean's surface) that was commonly observed at close range to the ship during high wind events, and at times, sidelobe contamination from intense nearby convection.

d. Comparisons to GATE convection

As alluded to in previous sections, comparisons of these results (i.e., number and rainfall contributions as a function of height, and rainfall rate as a function of height) to those obtained from GATE data must be made with some caution for a variety of reasons. First, some of the analyses of GATE data were performed on unpartitioned (no convective-stratiform separation) radar echoes (Houze and Cheng 1977). Second, distributions of radar echo, both unpartitioned and partitioned (Cheng and Houze 1979; Leary 1984), as a function of height and area are based on *maximum* heights and areas over the echo's lifetime, whereas this study is based on *instantaneous* heights (and areas, when dealing with convective features). Third, because of advances in automated analysis techniques, averages and distributions presented herein are generally based on longer, higher frequency, and contiguous datasets compared to GATE results. Despite these potential difficulties, comparing results from the GATE and COARE datasets is desirable for at least two reasons: 1) to evaluate the impact of analyzing instantaneous, convective-only echo distributions and 2) to determine if there are fundamental differences in the vertical structure of convection between the eastern Atlantic and western Pacific.

The effect of instantaneous versus maximum convective echoes on the distributions was first examined by plotting the frequency distributions of convective feature top heights in log-probability format (not shown), as was done in López (1977) and Houze and Cheng (1977) for unpartitioned radar echoes.[2] Both of these studies concluded that tropical echo top heights are approximately lognormally distributed, and begin to deviate from a lognormal distribution for heights greater than about 12 km. Results from the COARE dataset were also nearly lognormally distributed (passing the Chi-squared test for goodness of fit at the 95% confidence level) and even began to deviate from this distribution at the same height as the GATE echoes. Mean and standard deviations of the logarithms of height for both GATE and COARE are presented in Table 4 for comparison. The slightly higher means for COARE are most likely a result of the higher tropopause in the COARE region (approximately 16 km) versus that of GATE (about 13 km).

A second assessment of the effects of partitioning the data were made by examining the contribution to total convective area as a function of individual convective

[2] López (1977) presented log-probability distributions for convective echo from a variety of tropical locations, and Houze and Cheng (1977) presented distributions for the three phases of GATE.

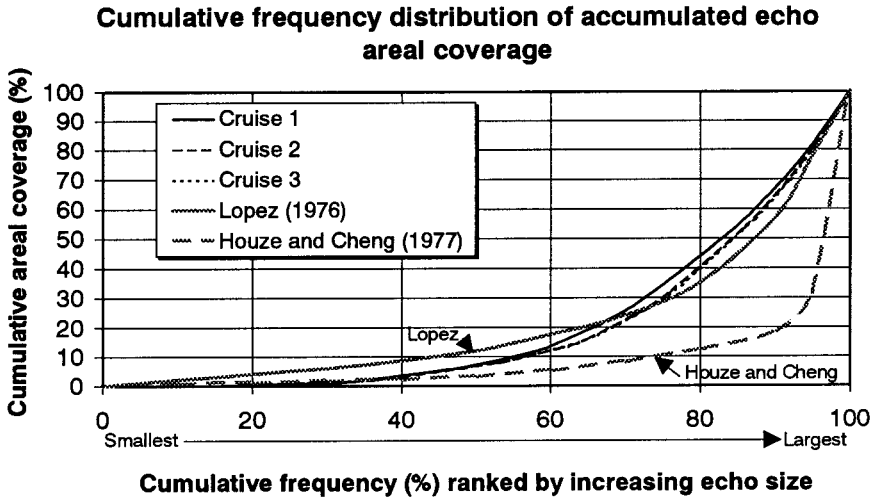

FIG. 16. Cumulative frequency distribution of accumulated echo areal coverage for Cruises 1, 2, and 3 (black lines). Results of similar analyses from Lopez (1976; solid gray line) and Houze and Cheng (1977; dashed gray line) are shown for comparison. See text for description of how the curves were determined.

area size. Cumulative frequency distributions of accumulated convective area as a function of feature area are presented in Fig. 16. The abscissa represents the percent of total convective features equal to or less than a given size bin. The ordinate represents the percent of total convective *area* represented by features equal to or smaller than the same size bin. Results of the same analysis from López (1977) and then Houze and Cheng (1977) (both based on maximum areas of unpartitioned echo) are plotted for comparison. In all three cases, the few most areally extensive echoes account for the bulk of total convective echo.

However, note that the COARE distributions are in close agreement to the López curve, while the Houze and Cheng curve lies farther to the right. As pointed out by Houze and Cheng (1977), the difference between the López and Houze and Cheng curves arises from differences in radar sensitivity. The radars used in GATE were more sensitive than those used in the López study, and therefore were able to detect greater amounts of weak stratiform echo, resulting in the tendency to connect separate regions of more intense echo into just a few very large echoes. The fact that the COARE results match those of López is a result of ''removing'' the interconnecting stratiform echo via the partitioning algorithm (which was well identified by the even more sensitive radars used in COARE).

Contributions to total convective rainfall as a function of feature height and comparisons to GATE results were discussed in section 3a. To the extent that long-term averages of instantaneous and maximum echo height distributions are similar, there do not appear to be significant differences between total convective rainfall production as a function of height for the two regions. It is of interest, however, to determine if rainfall rates as a function of echo top height are similar for the two regions. Because the COARE region is characterized by higher SSTs than the GATE region, boundary layer water vapor mixing ratios are higher in this region, which may result in different rainfall rate–cloud-top height relationships between the two regions. Although there is evidence of some differences during cruise 1 (Fig. 10), rainfall rates as a function of height for cruises 2 and 3 do not appear to differ significantly from those presented by Leary (1984) for GATE.[3] These results suggest that factors other than SST may have a greater impact on the rainfall rate–echo top height relationship, as is investigated in Part II.

4. Discussion

The analysis of section 3 revealed the following facts concerning the distribution of convective echo observed during the COARE IOP:

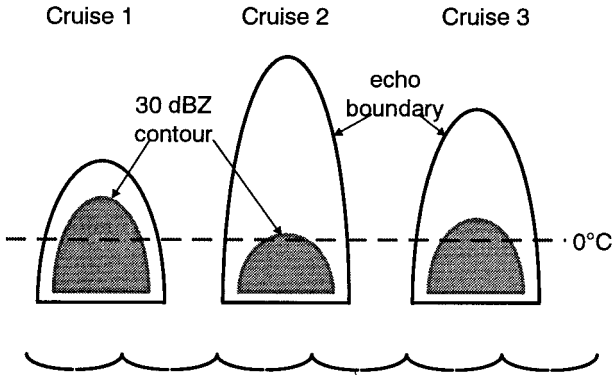

FIG. 17. Schematic illustration of the rain volume-weighted mean vertical structure of convection characteristic of each cruise of the R/V *Vickers.* Echo boundaries are indicated by black curves; 30-dB*Z* contours by gray curves. Regions of reflectivity greater than or equal to 30 dB*Z* are shaded. The approximate location of the freezing level with respect to the 30-dB*Z* contour height is shown as the dashed gray line. It is important to note that this figure represents averaging over time and weighting by rainfall production, thereby masking the large variability in convective vertical structure that was always present.

- On average, the shallowest convection, as measured by echo top height, occurred during cruise 1 and the deepest convection occurred during cruise 2. Cruise 3 echo top heights were intermediate.
- In terms of convective ''intensity,'' as measured by grid column 30-dB*Z* contour heights, cruises 1 and 2 had roughly the same percentage of tall 30-dB*Z* contour heights, with cruise 3 30-dB*Z* contour heights being slightly lower.
- Cruise 1 exhibited a somewhat bimodal rainfall distribution as a function of echo top height, whereas cruises 2 and 3 were unimodally distributed.
- Rainfall distributions as a function of 30-dB*Z* contour height reveal that proportionately more rainfall was produced by the tallest 30-dB*Z* contour heights during cruises 1 and 3 than by cruise 2. Despite the tall echo top heights observed during cruise 2, rainfall production was dominated by ''shorter'' 30-dB*Z* contour height columns.

Schematic illustrations of a ''mean'' convective core characteristic of each cruise are presented in Fig. 17. In constructing these figures, consideration was given to the relative amount of rain falling into each height bin. For example, even though the frequency distributions of 30-dB*Z* contour height were similar for cruises 1 and 2, the schematic 30-dB*Z* contour height in cruise 1 is higher than it is for cruise 2 since the taller 30-dB*Z* heights of cruise 1 rained proportionately more than those of cruise 2.

In this rainfall-weighted sense, the variations among convective echo top height and 30-dB*Z* contour height are evident. For example, although the convection of cruise 1 was relatively shallow, its internal structure was vertically intense, which is reflected both in terms of

[3] It should be noted, however, that Leary's results are based on only 25 h of data, taken from one of the most intense systems observed during GATE, so her results may not be strictly representative of mean conditions.

the height of the 30-dB*Z* contour as well as the slightly higher convective rainfall rates observed during cruise 1 (see Figs. 10 and 11). In contrast, the deep convection of cruise 2 was not particularly vertically intense, consistent with the lower mean surface rainfall rates observed during that cruise. It should be noted, however, that these schematic illustrations have no relation to the amount of rain that fell during any particular cruise or to the frequency of convection. In fact, despite the somewhat higher instantaneous convective rainfall rates observed during cruise 1, the least total amount of rain fell during this cruise, while the most rainfall occurred during cruise 2 (Rickenbach 1995).

The schematic illustration of convection observed during each cruise suggests that convection observed during cruise 1 was characterized by larger ice water concentrations above the freezing level than for cruises 2 and 3, which has consequently led to speculation as to what implications the vertical structure may have in terms of microphysical processes, vertical velocity characteristics, and diabatic heating profile shapes. In addition to vertical structure characteristics, the apparently inverse relation between convective intensity (i.e., convective rainfall rate and internal vertical structure) and total rainfall for each cruise raises questions concerning what environmental factors control each of these variables. Each of these questions is investigated in Part II of this study.

5. Summary

This study used nearly 90 days of radar data at 20-min resolution to examine the variability of the vertical structure of convection in the western Pacific warm pool region. Radar data were interpolated to a Cartesian grid and partitioned into convective and stratiform components. Distributions of the number of convective grid heights and 30-dB*Z* contour heights, as well as the convective rainfall contribution from each of these categories were examined. Shallow convection was more frequent and produced relatively more rainfall during cruise 1 than during cruises 2 or 3. However, when the distributions were based on ''internal structure,'' or 30-dB*Z* contour height, there was not much difference between the frequency distributions from cruise to cruise, emphasizing the fact that echo top height is only a partial indicator of convective intensity. This result was also confirmed in the ''two-dimensional'' distributions of convective echo, which revealed a wide range of 30-dB*Z* heights for a given echo top height. However, it is important to note that tall 30-dB*Z* contour heights contributed relatively more to total convective rainfall during cruises 1 and 3 than during cruise 2.

Consistent with previous studies, monthly mean rainfall rates increased with echo top height, and with 30-dB*Z* contour height. However, there is a significant amount of scatter about these mean values, particularly for echo top height. Instantaneous correlations (i.e., correlations computed for each radar volume analyzed) of the rainfall rate–echo top height and rainfall rate–30-dB*Z* contour height relationship reveal that rain-rate–echo top height correlations are nearly always lower than rain rate–30 dB*Z* contour height correlations. Furthermore, the rain rate–echo top height correlations are much more broadly distributed than the rain rate–30 dB*Z* contour height correlations, which are nearly always at least 0.7 or greater.

Schematic illustrations of the rainfall weighted mean convection sampled during each cruise illustrate that, although cruise 1 convection was shallow on average, it was vertically intense and rained heavily. In contrast, the deep convection of cruise 2 was not as vertically developed from an internal structure point of view and did not rain as heavily as its echo top heights might suggest. Convective characteristics of cruise 3 were situated between those of cruises 1 and 2 and tended to resemble the mean convective behavior of convection over the entire IOP.

Acknowledgments. Support for this work was provided by NASA Graduate Fellowship on Global Change NGT-30099 SUPP 3 and by NASA TRMM Grant NAG-5-2692. We gratefully acknowledge all of those who worked so hard before, during, and after COARE to make the shipboard radar program a success.

APPENDIX

Partitioning Radar Reflectivity Data into Convective and Stratiform Components

Using the gridded radar reflectivity data described in section 2, data are partitioned into convective and stratiform components using a technique based largely on that described by Steiner and Houze (1993). Their algorithm operates as follows: each data point on an *x*-*y* Cartesian grid is compared to the mean reflectivity of a ''background'' area. If the point in question is $\geq$40 dB*Z* (an ''absolute convective threshold''), then it and the points contained within the user-specified surrounding convective area are classified as convective. Furthermore, if the point in question does not exceed 40 dB*Z* but is $\geq$4.5 dB*Z* above the (linear) mean background reflectivity (which corresponds to a rainfall rate approximately twice that of the background area) then the point and all points within the convective area are tagged as convective. The convective echo is specified as a 10 km $\times$ 10 km grid box, while the background area is a 22 km $\times$ 22 km grid box. A schematic of the two areas is shown in Fig. A1. These sizes are determined prior to ''batch'' processing and do not vary during the partitioning process.

The single modification we have made to this algorithm lies in determining the ''absolute convective threshold.'' This modification was implemented in order to allow partitioning to take place at a variety of heights

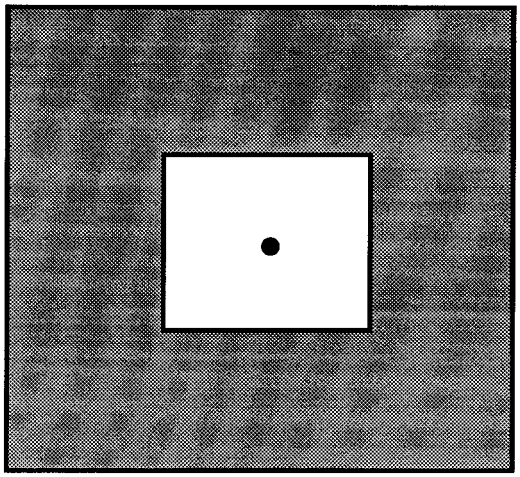

FIG. A1. Schematic illustration of the background area (large dark shaded box), convective area (smaller unshaded box), and data point being tested with the convective/stratiform partitioning algorithm (dot). If the point passes either of the two convective criteria (see text), it and all of the points in the convective area are designated as convective.

where, because of the decrease in reflectivity with height in convective cells, the 40-dB*Z* criterion was found to be too rigid. In our algorithm, for each radar volume being partitioned, the variable ''absolute convective'' threshold is determined by first constructing a contoured frequency by altitude diagram (CFAD) of radar reflectivity as described in Yuter and Houze (1995). A sample CFAD is shown in Fig. A2. The reflectivities at the rightmost extreme of the CFAD correspond to the most intense convective echo. We determined that the 2% frequency contour (on the right side of the distribution using 1-dB width reflectivity bins) was the best absolute convective threshold. This value was selected because it corresponded to core reflectivity values of the largest convective cells and produced the narrowest distribution of stratiform vertical velocities in the resulting stratiform partition. We applied the partitioning procedure described in the previous paragraph at the 2-km altitude, using the ''absolutely convective'' reflectivity threshold corresponding to the 2% contour at that same altitude.

REFERENCES

Adler, R. F., and R. A. Mack, 1984: Thunderstorm cloud height-rainfall rate relations for use with satellite rainfall estimation techniques. *J. Climate Appl. Meteor.,* **23,** 280–296.

——, and A. J. Negri, 1988: A satellite infrared technique to estimate tropical convective and stratiform rainfall. *J. Appl. Meteor.,* **27,** 30–51.

Arkin, P. A., and B. Meisner, 1987: The relationship between large-scale convective rainfall and cold cloud over the western hemisphere during 1982–1984. *Mon. Wea. Rev.,* **115,** 51–74.

Chen, S. S., R. A. Houze Jr., and B. E. Mapes, 1996: Multiscale variability of deep convection in relation to large-scale circulation in TOGA COARE. *J. Atmos. Sci.,* **53,** 1934–1945.

Cheng, C.-P., and R. A. Houze Jr., 1979: The distribution of convective and mesoscale precipitation in GATE radar echo patterns. *Mon. Wea. Rev.*, **107,** 1370–1381.

Cunning, J. B., 1988: Taiwan Area Mesoscale Experiment: Daily operations summary. NCAR Tech. Note, NCAR/TN-305+STR, 361 pp. [Available from the National Center for Atmospheric Research, Boulder, CO 80307.]

DeMaria, M., 1985: Linear response of a stratified tropical atmosphere to convective forcing. *J. Atmos. Sci.,* **42,** 1944–1959.

DeMott, C. A., R. Cifelli, and S. A. Rutledge, 1995: An improved method for partitioning radar data into convective and stratiform components. Preprints, *27th Conf. on Radar Meteorology,* Vail, CO, Amer. Meteor. Soc., 233–236.

Hartman, D. L., H. H. Hendon, and R. A. Houze Jr., 1984: Some implications of the mesoscale circulations in tropical cloud clusters for large-scale dynamics and climate. *J. Atmos. Sci.,* **41,** 113–121.

Holland, G. J., J. L. McBride, R. K. Smith, D. Jasper, and T. D. Keenan, 1986: The BMRC Australian Monsoon Experiment: AMEX. *Bull. Amer. Meteor. Soc.,* **67,** 1466–1472.

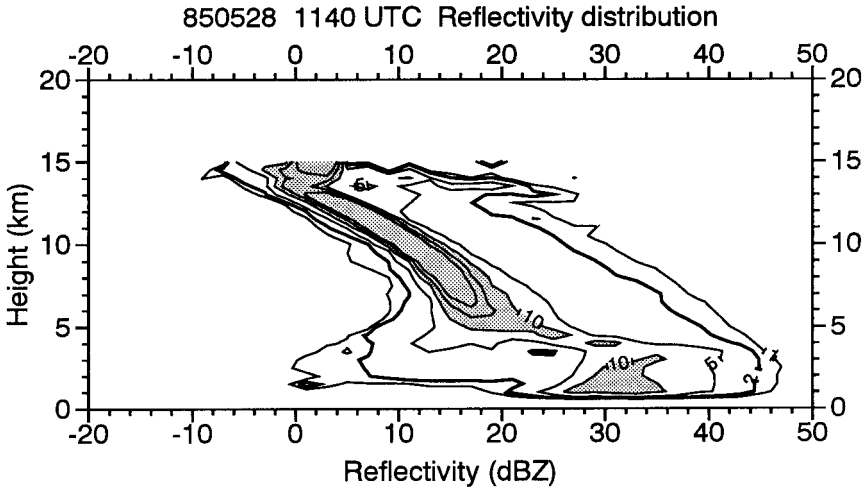

FIG. A2. CFAD of radar reflectivity for the 1140 UTC 28 May 1985 PRE-STORM case. The 2% relative frequency contour (drawn with a bold line) identifies the ''absolute convective'' reflectivity threshold for a given altitude.

Houze, R. A., Jr., 1989: Observed structure of mesoscale convective systems and implications for large-scale heating. *Quart. J. Roy. Meteor. Soc.*, **115,** 425–461.

——, and C.-P. Cheng, 1977: Radar characteristics of tropical convection observed during GATE: Mean properties and trends over the summer season. *Mon. Wea. Rev.*, **105,** 964–980.

Jorgensen, D. P., and M. A. LeMone, 1988: Taiwan Area Mesoscale Experiment: P-3 aircraft operations summary. NCAR Tech. Note, NCAR/TN-305+STR, 71 pp. [Available from the National Center for Atmospheric Research, Boulder, CO 80307.]

Kucera, P. A., D. A. Short, and O. W. Thiele, 1996: An analysis of rainfall intensity and vertical structure from shipborne radars in TOGA COARE. Preprints, *Seventh Conf. on Mesoscale Processes*, Reading, U.K., Amer. Meteor. Soc., 131–134.

Lau, K.-M., and L. Peng, 1987: Origin of low-frequency (intraseasonal) oscillations in the tropical atmosphere. Part I: Basic theory. *J. Atmos. Sci.*, **44,** 950–972.

Leary, C. A., 1984: Precipitation structure of the cloud clusters in a tropical easterly wave. *Mon. Wea. Rev.*, **112,** 313–325.

Lin, X., and R. H. Johnson, 1996: Kinematic and thermodynamic characteristics of the flow over the western Pacific warm pool during TOGA COARE. *J. Atmos. Sci.*, **53,** 695–715.

López, R. E., 1977: The lognormal distribution and cumulus cloud populations. *Mon. Wea. Rev.*, **105,** 865–872.

Madden, R. A., and P. R. Julian, 1994: Observations of the 40–50-day tropical oscillation—A review. *Mon. Wea. Rev.*, **122,** 814–837.

Petersen, W. A., S. A. Rutledge, and R. E. Orville, 1996: Cloud-to-ground lightning observations from TOGA COARE: Selected results and lightning location algorithms. *Mon. Wea. Rev.*, **124,** 602–620.

Rickenbach, T. M., 1995: Rainfall production from the spectrum of convection observed by shipboard radar during TOGA COARE. Preprints, *21st Conf. on Hurricanes and Tropical Meteorology*, Miami, FL, Amer. Meteor. Soc., 116–118.

——, and S. A. Rutledge, 1998: Convection in TOGA COARE: Horizontal scale, morphology, and rainfall production. *J. Atmos. Sci.*, **55,** 2715–2729.

Rutledge, S. A., E. R. Williams, and T. D. Keenan, 1992: The Down Under Doppler and Electricity Experiment (DUNDEE): Overview and preliminary results. *Bull. Amer. Meteor. Soc.*, **73,** 3–16.

——, R. Cifelli, C. DeMott, W. Petersen, T. Rickenbach, J. Lutz, R. Bowie, M. Strong, and E. Williams, 1993: The shipboard deployment of the MIT C-band radar during TOGA COARE. Preprints, *26th Int. Conf. on Radar Meteorology*, Amer. Meteor. Soc., Norman, OK, 371–373.

Steiner, M., and R. A. Houze Jr., 1993: Three-dimensional validation at TRMM ground truth sites: Some early results from Darwin, Australia. Preprints, *26th Int. Conf. on Radar Meteorology*, Amer. Meteor. Soc., Norman, OK, 417–420.

——, R. A. Houze Jr., and S. E. Yuter, 1995: Climatological characterization of three-dimensional storm structure from operational radar and rain gauge data. *J. Appl. Meteor.*, **34,** 1978–2007.

Szoke, E. J., E. J. Zipser, and D. P. Jorgensen, 1986: A radar study of convective cells in mesoscale systems in GATE. Part I: Vertical profile statistics and comparison with hurricanes. *J. Atmos. Sci.*, **43,** 181–197.

Tao, W.-K., J. Simpson, S. Lang, M. McCumber, R. Adler, and R. Penc, 1990: An algorithm to estimate the heating budget from hydrometeor distributions. *J. Appl. Meteor.*, **29,** 1232–1244.

Tokay, A., and D. Short, 1996: Evidence from tropical raindrop spectra of the origin of rain from stratiform versus convective clouds. *J. Appl. Meteor. Sci.*, **35,** 355–371.

Webster, P. J., and R. A. Houze Jr., 1991: The Equatorial Mesoscale Experiment (EMEX): An overview. *Bull. Amer. Meteor Soc.*, **72,** 1481–1505.

——, and R. Lukas, 1992: TOGA COARE: The coupled ocean–atmosphere response experiment. *Bull. Amer. Meteor. Soc.*, **73,** 1377–1417.

Williams, E., and N. Renno, 1993: An analysis of conditional instability of the tropical atmosphere. *Mon. Wea. Rev.*, **121,** 21–36.

Yuter, S. E., and R. A. Houze Jr., 1995: Three-dimensional kinematic and microphysical evolution of Florida cumulonimbus. Part II: Frequency distributions of vertical velocity, reflectivity, and differential reflectivity. *Mon. Wea. Rev.*, **123,** 1941–1963.

Zipser, E. J., 1994: Deep cumulonimbus cloud systems in the Tropics with and without lightning. *Mon. Wea. Rev.*, **122,** 1837–1851.

——, and K. R. Lutz, 1994: The vertical profile of radar reflectivity of convective cells: A strong indicator of storm intensity and lightning probability? *Mon. Wea. Rev.*, **122,** 1751–1759.